Sensors & Diagnostics

PAPER

View Article Online
View Journal | View Issue

Cite this: *Sens. Diagn.*, 2023, **2**, 457

Microfluidic concurrent assessment of red blood cell adhesion and microcapillary occlusion: potential hemorheological biomarkers in sickle cell disease†

Yuncheng Man ‡§[a] Douglas H. Wu,§[a] Ran An, §[a] Peiran Wei,[b] Karamoja Monchamp,[ac] Utku Goreke, [a] Zoe Sekyonda,[d] William J. Wulftange, [d] Chiara Federici,[ce] Allison Bode,[ac] Lalitha V. Nayak,[c] Jane A. Little[f] and Umut A. Gurkan *[adg]

Deformability and non-adherence are two fundamental functional properties of red blood cells (RBCs), which allow them to move unimpeded through the microvasculature. In sickle cell disease (SCD), polymerization of abnormal sickle hemoglobin leads to decreased deformability and increased membrane adhesiveness in RBCs. This contributes to abnormal blood vessel occlusion, which is central to the underlying pathophysiology. RBC deformability and adhesiveness are, therefore key hemorheological biomarkers in characterizing disease states as well as in evaluating novel therapeutics. To date, these important interrelated biomarkers have been assessed in distinct laboratory assays, without integration or concurrent assessment *in vitro*. To this end, we present a novel microfluidic assay in which laminin (LN, a sub-endothelial matrix protein that mimics microvascular damage and extracellular matrix exposure)-functionalized microcapillaries ranging from 20 μm to 4 μm are embedded in microchannels, for simultaneous assessment of microcapillary occlusion mediated by RBC deformability and vascular cellular adhesion mediated by pathologic RBC membrane changes. We show that RBC adhesion to LN or microcapillary occlusion can be associated with markers for intravascular hemolysis or iron overload in SCD. Following allogeneic hematopoietic stem cell transplant (HSCT), which is a curative therapy, in a single subject with SCD, RBC-mediated microcapillary occlusion fell into the healthy range, but RBC adhesion to LN, albeit significantly decreased, remained outside the healthy range. Our findings demonstrate the potential of this bifunctional assay, in both monitoring the clinical course and supplementing clinical observations with comprehensive evaluation of two functional hemorheological properties.

Received 27th May 2022,
Accepted 18th January 2023

DOI: 10.1039/d2sd00095d

rsc.li/sensors

Introduction

Red blood cells (RBCs) are one of the major cellular components of blood and are the primary means of oxygen delivery throughout the circulatory system.[1] Mature RBCs lack a nucleus and organelles, primarily relying on the cell membrane for their functional properties.[2] It was first shown in 1675 that RBCs flexibly pass through narrow capillaries by deforming into ovals and thereafter resuming a round shape when transiting larger vessels.[3] This exceptional flexibility is accomplished by optimal membrane structural organization, a large surface area-to-volume ratio, high membrane viscoelasticity, low cytoplasmic viscosity, and low expression of adhesive molecules on the membrane.[4–6] RBCs are generally considered deformable and non-adherent; however, in the inherited blood disorder, sickle cell disease (SCD), RBC

[a] *Department of Mechanical and Aerospace Engineering, Case Western Reserve University, 10900 Euclid Ave., Cleveland, OH 44106, USA. E-mail: umut@case.edu*
[b] *Soft Matter Facility, Texas A&M University, College Station, TX, USA*
[c] *Division of Hematology and Oncology, School of Medicine, Case Western Reserve University, Cleveland, OH, USA*
[d] *Department of Biomedical Engineering, Case Western Reserve University, Cleveland, OH, USA*
[e] *BioChip Labs, Inc., Cleveland, OH, USA*
[f] *Department of Hematology, UNC Blood Research Center, School of Medicine, University of North Carolina, Chapel Hill, NC, USA*
[g] *Case Comprehensive Cancer Center, Case Western Reserve University, Cleveland, OH, USA*

† Electronic supplementary information (ESI) available. See DOI: https://doi.org/10.1039/d2sd00095d

‡ Current address: Wyss Institute for Biologically Inspired Engineering at Harvard University, Boston, MA, USA.

§ These authors contributed equally to this work.

deformability notably decreases and adhesiveness increases due to polymerization of abnormal sickle hemoglobin (HbS) and enhanced expression of molecules.[7,8] These adhesive molecules include very late antigen-4 (VLA-4) and CD36 on 'stress' reticulocytes,[9,10] and intercellular adhesion molecule-4 (ICAM-4) and basal cell adhesion molecule-1/Lutheran (BCAM/Lu) on mature sickle RBCs.[11,12] Adhesion and microcapillary occlusion, caused by increased RBC adhesiveness and decreased RBC deformability, are two major contributors to pathophysiology in SCD. Reliable measurement of these two functional hemorheological properties will significantly improve our understanding of disease pathogenesis and of the impact of novel therapies.

Conventionally, cellular deformability or adhesion is measured at a single-cell level by micropipette aspiration,[13–15] atomic force microscopy,[16–19] or optical trapping.[20–22] However, these techniques are labor intensive and require skilled operators, which significantly limit their throughput for assessing large quantities of cells in clinical studies. Bulk techniques, such as microfiltration and passive wash assays, have been developed.[23–25] However, the microfiltration technique is prone to clogging, and the passive wash assay lacks flow shear, which may bias the results. In current clinical laboratory settings, RBCs are typically analyzed by ektacytometry,[26–29] or in microfluidic channels lined with endothelial cells or functionalized with endothelial-associated proteins.[30–36] Ektacytometry provides a bulk average, and therefore it is limited by its ability to measure deformability of individual cells.[28] Microchannels designed for adhesion measurement are typically at least one order of magnitude larger than the red cell dimension (>50 μm) and therefore present limitations in providing measurement of RBCs perfusing through microcapillaries. Both RBC adhesion and RBC-mediated microcapillary occlusion are the root causes of microvascular complications in SCD, which makes individual laboratory measurements challenging and less informative. Therefore, there is a strong impetus to develop a technique for assessing these two important hemorheological biomarkers in a concurrent manner *in vitro*.

Microfluidic vascular networks molded in polydimethylsiloxane (PDMS) elastomers have been used for investigation of RBC-mediated microcapillary occlusion.[37–39] While these microfluidic technologies greatly simplify analysis, they were not used to assess RBC adhesion due to a lack of endothelial-associated adhesion molecules. The concept of coating PDMS microfluidic microcapillary networks with proteins was previously introduced.[40] However, the previous work adopted microfluidic dimensions greater than 10 μm (larger than typical capillary dimensions) which is not feasible for RBC deformation measurement. Further, the protein coating was achieved by physical adsorption, which carries a 'protein rubbing-off' risk, and thereby low experimental reproducibility. More recently, Lu *et al.* carried out surface chemistry for covalent protein functionalization in microchannels,[41] but reported a perfusion rate, which is not a direct indicator of adhesion or microcapillary occlusion. To address the technical limitation, here we describe a functionalized OcclusionChip assay that enables concurrent assessment of RBC adhesion and RBC-mediated microcapillary occlusion. The OcclusionChip consists of a gradient of microcapillary arrays, from 20 to 4 μm, with two 60 μm side channels mimicking vascular networks and arteriovenous anastomoses in the capillary bed.[42] We chose to functionalize the microchannel with human laminin (LN), a sub-endothelial extracellular matrix protein exposed on activated endothelium and damaged microvascular endothelium, which adheres to sickle RBCs, a key mechanism contributing to vaso-occlusion in SCD.[43] We show that implementation of the functionalized OcclusionChip assay, which assays two functional hemorheological biomarkers in SCD, could allow integrated characterization of the clinical course, even in the absence of clinical laboratory tests, and a more comprehensive evaluation of novel therapies.

Materials and methods

Microfluidic device

Fig. 1 shows the design, mechanism, and operation of the functionalized OcclusionChip assay. As described previously,[44] the OcclusionChip consists of nine micropillar arrays forming uniform microcapillaries within each array but overall finer microcapillaries along the flow direction from 20 μm down to 4 μm, coupled with two 60 μm side passageways (Fig. 1A). The microfluidic microcapillary networks recreate the non-uniform, continuously changing capillary bed, and the microfluidic anastomoses help regulate the blood flow for prevention of upstream clogging.[45,46] The microchannel surface was also functionalized with LN. Therefore, flowing abnormal RBCs may obstruct the microcapillaries or adhere to the microchannel surface (Fig. 1B and inset). LN was covalently immobilized on the top and side polydimethylsiloxane (PDMS) wall and the bottom glass wall through different surface chemistry mechanisms for RBC adhesion measurement (Fig. 1C and D).[47–51] A photograph of the OcclusionChip blood test is shown in Fig. 1E. Disposable single-use microfluidic devices prevented cross-contamination between blood samples.

The OcclusionChip devices were fabricated using standard soft photolithography protocols (Fig. S1†). Briefly, a master silicon wafer was fabricated by UV-micropatterning a uniform SU8-2010 (Microchem, Newton, MA) photoresist layer with the layout of the microfluidic device. The surface of the master wafer was then passivated with triethoxy(1*H*,1*H*,2*H*,2*H*-perfluoro-1-octyl)silane (Sigma Aldrich, St. Louis, MO). Degassed PDMS (Sylgard 184, Dow Corning Corp, Midland, MI) (at 1 : 10 curing agent to liquid PDMS) was cast on top of the silicon wafer and cured at 80 °C overnight. The PDMS replicas were punched with 0.5 mm-diameter ports for inlets and outlets, and bonded to microscope glass slides (Gold Seal adhesion slides, adhesion coating: 3-aminopropyl triethoxysilane (APTES), Electron Microscopy Sciences, Hatfield, PA) through oxygen plasma treatment.

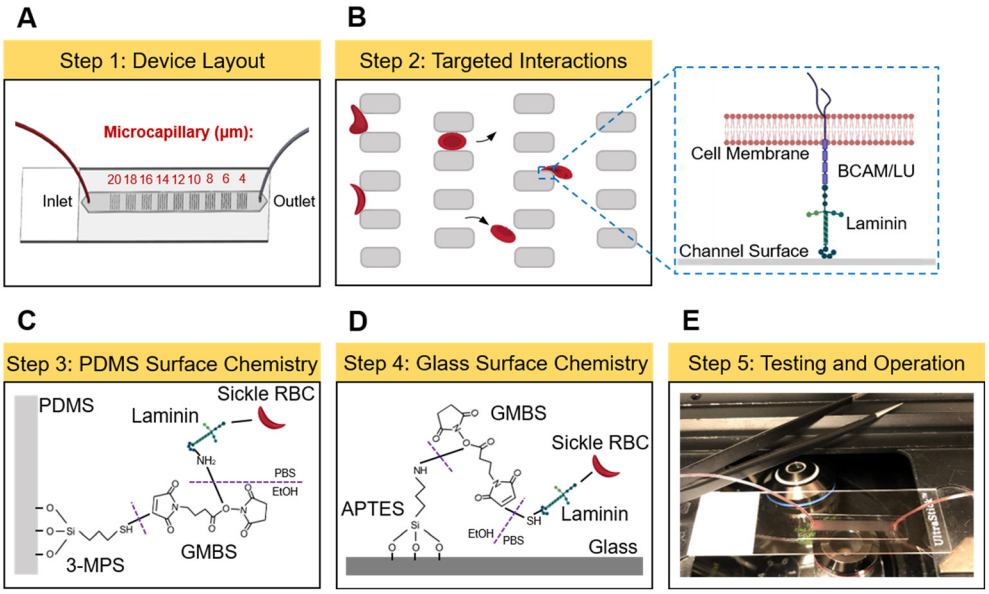

Fig. 1 Microfluidic device design, surface chemistry, and operation. (A) Schematics of the OcclusionChip device featuring the gradient of microcapillary networks from 20 μm down to 4 μm along the flow direction. (B) Laminin (LN) functionalization and the microcapillary networks enable concurrent assessment of red blood cell (RBC) adhesion on LN and RBC-mediated microcapillary occlusion. (C and D) Surface chemistry mechanisms of LN functionalization. (E) The new functionalized OcclusionChip assay tests clinical blood samples.

Laminin functionalization

For LN-functionalized microchannels, (3-mercaptopropyl) trimethoxysilane (3-MPS, Sigma Aldrich) working solution was prepared by diluting the stock solution in pure ethanol at 2%. *N*-γ-Maleimidobutyryl-oxysuccinimide ester (GMBS, ThermoFisher Scientific, Waltham, MA) was prepared by dissolving 25 mg of GMBS in 0.25 mL dimethyl sulfoxide (DMSO) and diluting with pure ethanol at 0.28% volume ratio. Human placental LN (laminin-511, Sigma Aldrich) was diluted in phosphate-buffered saline (PBS, 1×, pH = 7.4) at the final concentration of 25 μg mL^{-1}. Bovine serum albumin (BSA, ProSpec-Tany TechnoGene Ltd., East Brunswick, NJ) solution was prepared by dissolving 20 mg of lyophilized BSA in 1 mL PBS. After tubing assembly, the microchannels were initially rinsed with pure ethanol, incubated with 3-MPS working solution for 15 min at room temperature (RT), and rinsed again with pure ethanol. Next, the microchannels were incubated with GMBS working solution for 15 min at RT, followed by rinsing with pure ethanol and PBS. Thereafter, LN solution was injected into the microchannels and incubated for 90 min at RT, and then blocked with BSA. Non-functionalized microchannels were prepared similarly, but were incubated with PBS only for 90 min at RT. All microchannels were stored at 4 °C overnight before use. Prior to microfluidic experiments, the microchannels were rinsed with PBS.

Surface characterization

For surface characterization, we treated virgin PDMS substrates same as the microfluidic channel (before introducing LN) and performed contact angle measurement and attenuated total reflectance-Fourier transform infrared (ATR-FTIR) spectroscopy. Non-treated PDMS was used as a control. The contact angle was measured with a contact angle goniometer (Ramé-Hart Instrument Co., Succasunna, NJ) using the sessile drop method, where the value was obtained using the tangent fit method. Each value reported here is one measurement of one drop of water on the substrate. Three drops of water were measured on individual substrates and three substrates were measured in each condition. The ATR-FTIR experiment was carried out by using an FT/IR-4600 spectrometer (Jasco Inc., Easton, MD) with a ZnSe/diamond prism and an angle of incidence of 45°. The spectra were recorded from 4000 to 500 cm^{-1} with a resolution of 2 cm^{-1} and a data interval of 0.482 cm^{-1} (7261 data points in total for each experiment). One PDMS substrate was measured for each condition.

Fluorescence labeling of laminin and confocal imaging

To verify the surface functionalization approach, following BSA blocking, an Alexa Fluor 488 conjugated anti-human LN antibody (Novus Biologicals, Littleton, CO) at 1 : 100 v/v dilution in PBS was introduced into a non-functionalized and a LN-functionalized microchannel, and was incubated for 30 min at RT in the dark. Thereafter, the microchannels were rinsed with PBS and were imaged using a Leica TCS SP8 STED 3× system. A stack of images in the same field of view but varying focal distances were obtained and were projected onto a 2D plane by maximum intensity projection for both microchannels.

Blood sample acquisition

De-identified venous blood samples were drawn from non-anemic healthy controls (HbAA) and subjects with homozygous SCD (HbSS) or SCT (HbAS) into ethylenediaminetetraacetic acid (EDTA)-containing vacutainers at University Hospitals Cleveland

Medical Center (UHCMC) in Cleveland, Ohio under Institutional Review Board (IRB)-approved protocols (05-14-07C). Informed consent was obtained from all study participants. The blood samples were stored at 4 °C till tested. All experiments in this study were performed within 24 h of venipuncture. The clinical variables of the subjects with SCD, including the ARC, LDH, hemoglobin level, RBC count, hematocrit, ferritin level, white blood cell (WBC) count, absolute neutrophil count (ANC) and platelet count, were extracted from the medical records. Hb compositions, including HbS, HbA and HbF, as well as their fractions, were obtained through high-performance liquid chromatography (HPLC) at UHCMC.

Microfluidic experiments

Whole blood samples were centrifuged at 500*g* for 5 min at RT, after which the plasma and buffy coat were carefully removed. The pellet RBCs were washed twice in PBS and re-suspended in PBS at 20% hematocrit. A Flow-EZ™ microfluidic flow control system (Fluigent, Lowell, MA) was used to regulate the flow in the experiments (Fig. S2†). Briefly, the RBC suspension was loaded into the sample reservoir and was allowed to perfuse at 35 mbar for 20 min, which was followed by post-perfusion PBS washing for 20 min. An Olympus IX83 inverted motorized microscope with Olympus Cell Sense live-cell imaging and analysis software was used to obtain microscopy phase-contrast images upon the conclusion of the post-perfusion washing step. The images were further processed using Adobe Photoshop software (San Jose, CA).

Quantification of adherent RBCs and the occlusion index

To effectively compare the results of different blood samples, the number of adherent RBCs within the area of interest (AOI), which was defined as the entire region of the 4 μm to 10 μm microcapillary arrays (since the typical capillary dimension is less than 10 μm), was quantified and reported. The number of microcapillary occlusions was also quantified within the AOI, after which the occlusion index (OI), an intuitive generalizable parameter representing the overall microcapillary network occlusion percentage as previously described (Fig. S3†), was quantified and reported.

Statistical analysis

Data were reported as mean ± standard deviation (SD) in this study. Data were initially analyzed for normality, followed by appropriate two-group analyses: the unpaired *t*-test if data in both groups are normally distributed, and the Mann–Whitney *U* test if data in one of the two groups are non-normal.[52–54] Simple linear regression was used to assess the correlation between measurements and clinical variables, and the coefficient of determination R^2 was reported. Statistical significance was defined with *P*-values less than 0.05 ($P < 0.05$). All statistical analyses were carried out using GraphPad Prism software (GraphPad Software, Inc., San Diego, CA).

Results

Characterization of PDMS surfaces

To validate the surface chemistry for LN functionalization on the PDMS surface, control PDMS substrates and chemically modified PDMS substrates were initially investigated by using contact angle measurement. We found that following surface treatment, the wettability of the PDMS substrates significantly increased (Fig. S4A,† 68 ± 3° *vs.* 102 ± 1° for modified *vs.* control, $P < 0.001$, Mann–Whitney). The chemical structure of the PDMS surfaces was then characterized with ATR-FTIR, as shown in Fig. S4B.† A previous study suggested that the decrease of the bands around 2.8 to 3×10^3 cm^{-1} was caused by oxidation of methyl and methylene groups, and the increase of the bands around 1×10^3 cm^{-1} was caused by generation of some polar oxygen-containing functional groups, including alcohols and carboxylic acids.[55] These polar functional groups at the PDMS surface potentially interact with LN proteins for surface functionalization.

Validation of laminin functionalization

The projected image obtained from the LN-functionalized microchannel using confocal imaging had significantly greater fluorescence intensity than that from the non-functionalized microchannel (Fig. S5†). We further tested RBC samples from 6 HbSS subjects in both LN-functionalized and non-functionalized microchannels. Fig. 2A shows the representative microscopy images of RBC adhesion and microcapillary occlusion obtained from a single HbSS subject. When comparing results from LN-functionalized microchannels and those from non-functionalized microchannels, no difference was observed in the OI (Fig. 2B, $P = 0.6645$ (no significance), Mann–Whitney), but a significantly greater number of adherent RBCs was observed in LN-functionalized microchannels than in non-functionalized microchannels (Fig. 2C, $8.3 \pm 5.6 \times 10^2$ *vs.* $0.3 \pm 0.3 \times 10^2$, $P = 0.0058$, unpaired *t* test). Taken together, these data show that LN was effectively functionalized on the microchannel surface.

Process reproducibility

To validate the process reproducibility, we tested one RBC sample obtained from a single HbSS subject using 4 LN-functionalized devices manufactured from different batches. The OI was quantified to be 4.2 ± 0.8%, and the number of adherent RBCs was $4.2 \pm 1.0 \times 10^2$ (Fig. S6†). These data show that the experimental process yields consistent results.

Microfluidic concurrent assessment of RBC adhesion and microcapillary occlusion in SCT and SCD

To demonstrate the clinical utility of the present assay, we tested RBC samples from 4 healthy controls (HbAA), 5 subjects with SCT (HbAS), and 18 subjects with SCD (HbSS). Fig. 2D shows the representative microscopy images of RBC adhesion and microcapillary occlusion obtained from three subjects, one

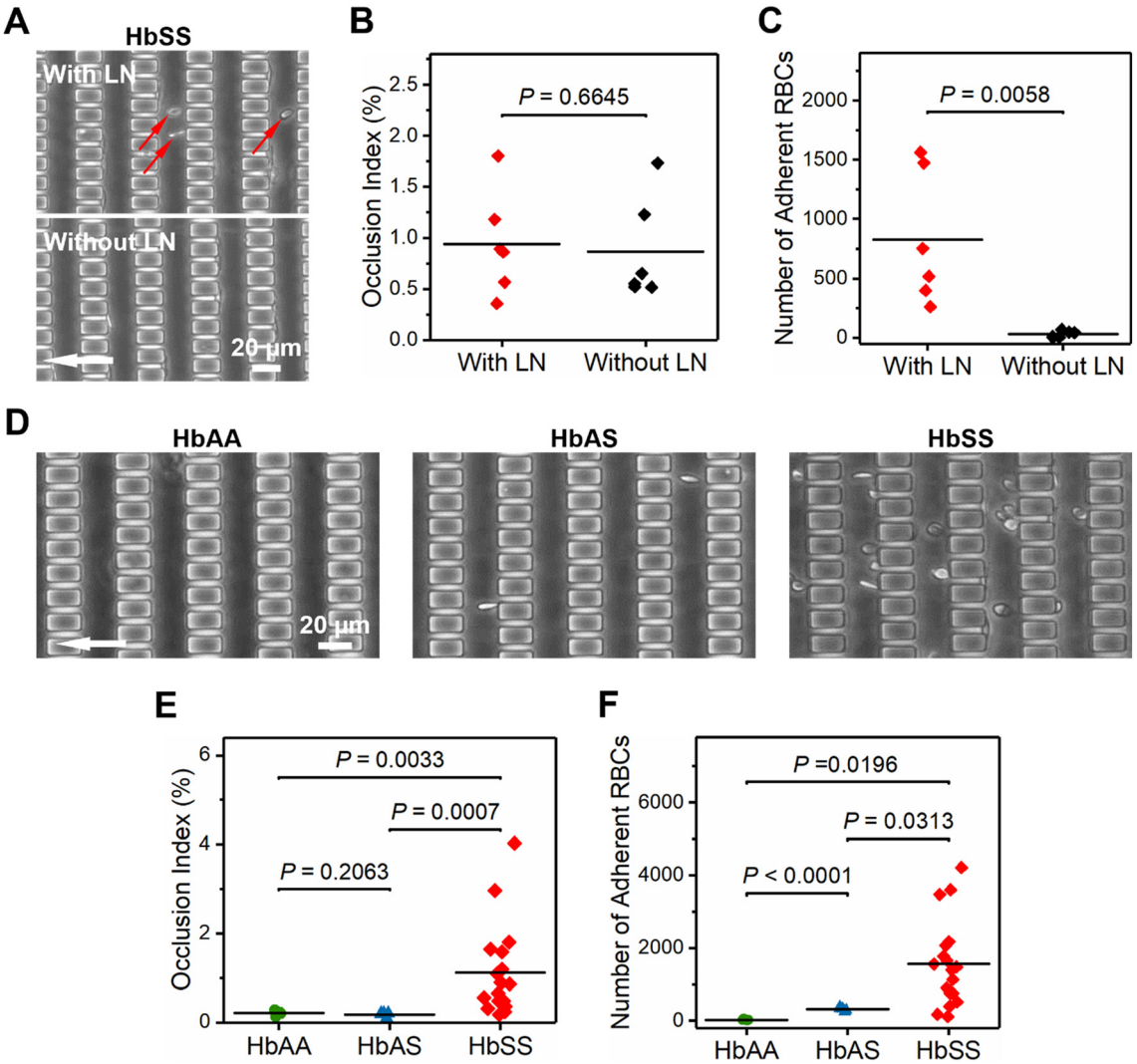

Fig. 2 Microfluidic concurrent assessment of RBC adhesion on laminin (LN) and microcapillary occlusion in sickle cell trait (SCT) and homozygous sickle cell disease (SCD). (A) Representative microscopy images showing RBC adhesion and microcapillary occlusion from a single HbSS subject tested in a LN-functionalized microchannel and a non-functionalized microchannel. Adherent RBCs are indicated with red arrows. (B) No difference in the occlusion index (OI) was observed when comparing microchannels with and without LN in the 6 tested HbSS subjects ($P = 0.6645$, Mann–Whitney). (C) The number of adherent RBCs was significantly greater in the LN-functionalized microchannels than in the non-functionalized microchannels for the 6 tested HbSS subjects ($P = 0.0058$, unpaired t test). (D) Representative microscopy images showing RBC adhesion and microcapillary occlusion in a healthy subject (HbAA), a subject with SCT (HbAS), and a subject with SCD (HbSS) in LN-functionalized microchannels. (E) Subjects with HbSS had significantly greater OI values than subjects with HbAA or HbAS ($P = 0.0033$ or $P = 0.0007$, Mann–Whitney). (F) Subjects with HbSS had a significantly greater number of adherent RBCs than subjects with HbAA or HbAS ($P = 0.0196$ or $P = 0.0313$, unpaired t test). Further, subjects with HbAS had a significantly greater number of adherent RBCs than subjects with HbAA ($P < 0.0001$, unpaired t test).

from each of the three cases. We observed negligible microcapillary occlusion in samples from subjects with HbAA or HbAS; however, we found considerable occlusion in samples from subjects with HbSS, which yielded a significantly greater OI than from those with HbAA and HbAS (Fig. 2E, 1.1 ± 1.0% *vs.* 0.2 ± 0.1% for HbSS *vs.* HbAA, and *vs.* 0.2 ± 0.1% for *vs.* HbAS, $P = 0.0033$ and $P = 0.0007$, Mann–Whitney). Moreover, we found that the number of adherent RBCs is significantly greater in samples from subjects with HbSS than from those with HbAA or HbAS (Fig. 2F, $1.6 \pm 1.2 \times 10^3$ *vs.* $0.3 \pm 0.1 \times 10^2$ for HbSS *vs.* HbAA, and *vs.* $3.2 \pm 0.5 \times 10^2$ for *vs.* HbAS, $P = 0.0196$ and $P = 0.0313$, unpaired t test). Interestingly, we also found that the number of adherent RBCs is significantly greater in samples from subjects with HbAS than from those with HbAA (Fig. 2F, $P < 0.0001$, unpaired t test). Altogether, these data suggest that RBC deformability in SCT is comparable to the healthy but is significantly decreased in SCD. Further, RBC adhesion is significantly enhanced in SCD, and is slightly enhanced in SCT.

Association of RBC adhesion to LN and OI with clinical markers for vascular hemolysis and iron overload in SCD

We next analyzed the associations between our measurements and clinical variables in 18 subjects with

homozygous SCD. We initially assessed hemolytic biomarkers, including the ARC, LDH, Hb level, RBC count and hematocrit, and a biomarker for iron overload, ferritin. We found that the OI is significantly associated with the ARC (Fig. 3A, R^2 = 0.5546, P = 0.0004) and LDH level (Fig. 3B, R^2 = 0.3022, P = 0.0181), but not with the Hb level (Fig. 3C, R^2 = 0.1655, P = 0.0939), RBC count (Fig. 3D, R^2 = 0.2133, P = 0.0537), hematocrit (Fig. 3E, R^2 = 0.1641, P = 0.0954) or ferritin level (Fig. 3F, R^2 = 0.2010, P = 0.0620). Meanwhile, we found that RBC adhesion to LN is significantly associated with the ARC (Fig. 3G, R^2 = 0.5760, P = 0.0003) and LDH level (Fig. 3H, R^2 = 0.2419, P = 0.0382), but not with the Hb level

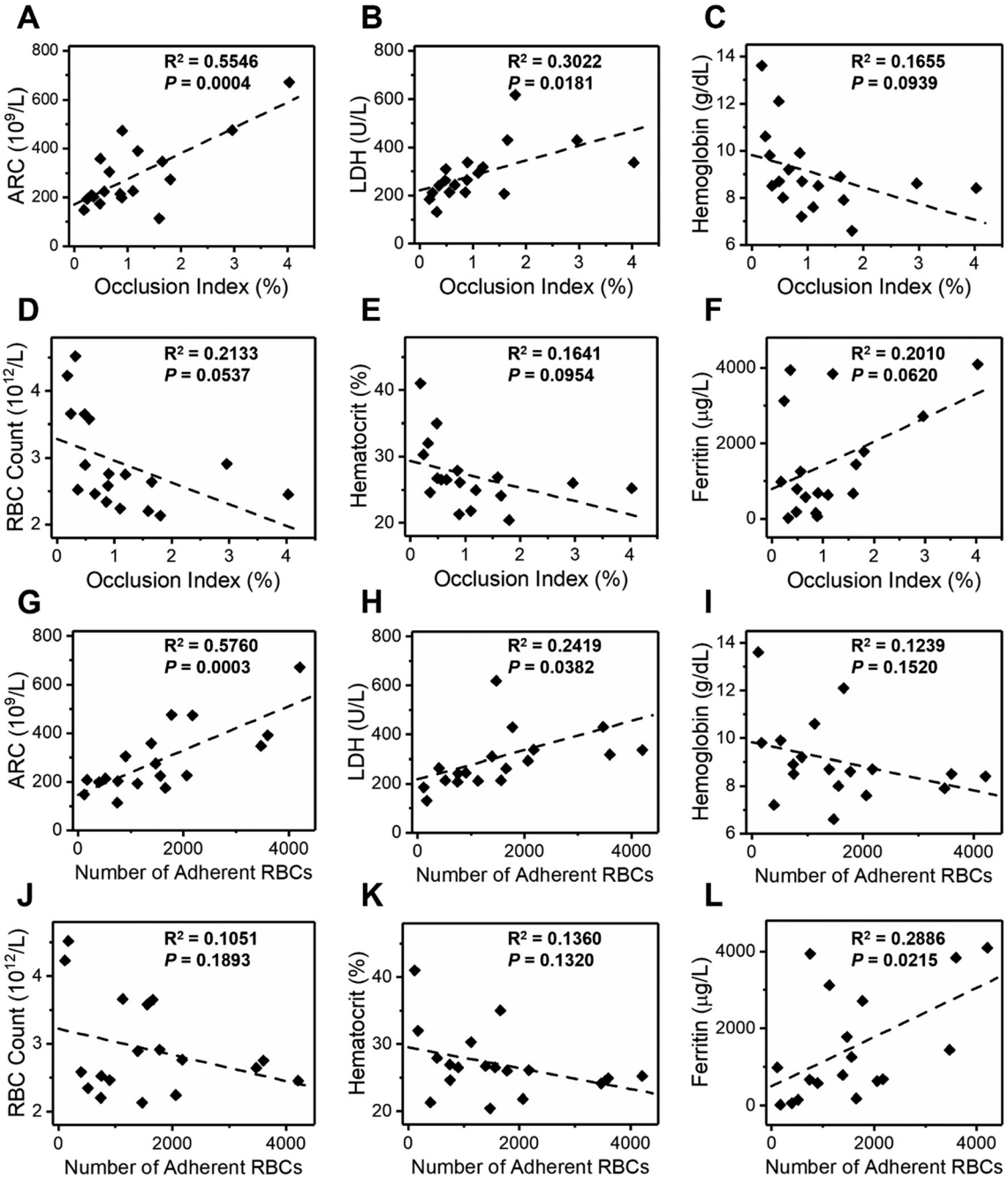

Fig. 3 Association of RBC adhesion to laminin (LN) and occlusion index (OI) with clinical biomarkers for vascular hemolysis and iron overload in SCD. In the 18 study subjects with HbSS, the OI is significantly associated with the (A) absolute reticulocyte count (ARC) (R^2 = 0.5546, P = 0.0004) and (B) lactate dehydrogenase (LDH) level (R^2 = 0.3022, P = 0.0181), but not with the (C) hemoglobin level (R^2 = 0.1655, P = 0.0939), (D) RBC count (R^2 = 0.2133, P = 0.0537), (E) hematocrit level (R^2 = 0.1641, P = 0.0954) or (F) ferritin level (R^2 = 0.2010, P = 0.0620). Moreover, the number of adherent RBCs is significantly associated with the (G) ARC (R^2 = 0.5760, P = 0.0003) and (H) LDH level (R^2 = 0.2419, P = 0.0382), but not with the (I) hemoglobin level (R^2 = 0.1239, P = 0.1520), (J) RBC count (R^2 = 0.1051, P = 0.1893) or (K) hematocrit (R^2 = 0.1360, P = 0.1320). (L) The number of adherent RBCs is significantly associated with the ferritin level (R^2 = 0.2886, P = 0.0215).

(Fig. 3I, R^2 = 0.1239, P = 0.1520), RBC count (Fig. 3J, R^2 = 0.1051, P = 0.1893), or hematocrit (Fig. 3K, R^2 = 0.1360, P = 0.1320). Notably, we found that RBC adhesion to LN is significantly associated with the ferritin level (Fig. 3L, R^2 = 0.2886, P = 0.0215). These data suggest that samples from subjects with SCD showing more RBC adhesion or microcapillary occlusion are more likely to have signs of hemolysis or iron overload in SCD.

We found no associations between our measurements and Hb compositions including HbS, HbA, and HbF (Fig. S7†), or inflammatory biomarkers including WBC count, ANC, and platelet count (Fig. S8†). In the 18 study HbSS subjects, 8 were on transfusion therapy, 4 were on hydroxyurea, 1 was on Endari, 1 received allogeneic hematopoietic stem cell transplant (HSCT), and 4 were on supportive care (absence of disease-modifying therapies). In this modest number of subjects, we did not observe any differences amongst treatment groups (Fig. S9†). Table S1† summarizes the clinical data of the study population with SCD and our findings.

Microfluidic concurrent assessment of RBC adhesion and microcapillary occlusion in a subject with SCD before and after allogeneic hematopoietic stem cell transplant

We tested blood samples acquired from a subject with HbSS 57 days prior to and 81 days post receiving allogeneic HSCT. The donor genotype is HbAS and chimerism analysis 102 days post treatment shows that the recipient DNA accounted for less than 1% of total DNA. Our results show that the OI decreased by 68% and fell into the healthy range, following the treatment (Fig. 4A, 0.2% *vs.* 0.6%, healthy range: 0–0.2%). Although the number of adherent RBCs on LN decreased by 56% following the treatment, it is still above the healthy range (Fig. 4B, 1.2 *vs.* 2.6 × 10^2, healthy range: 0.0–0.2 × 10^2), suggesting that the subject may still develop abnormal vascular complications post treatment. Medical records also show that the subject had pain-related acute care clinic visits post treatment.

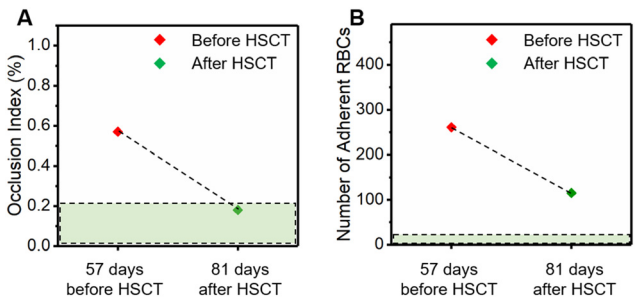

Fig. 4 Concurrent assessment of RBC adhesion to laminin (LN) and microcapillary occlusion of a subject with HbSS prior to and post allogeneic hematopoietic stem cell transplant (HSCT), which is a curative therapy for SCD. (A) The OI and (B) the number of adherent RBCs to LN significantly decreased following the treatment. The green dashed rectangular zones denote the healthy range of the measurements.

Discussion

Data reported in this study suggest that the new OcclusionChip assay integrated with surface chemistry provides a functional, reproducible *in vitro* approach for concurrent assessment of RBC adhesion and microcapillary occlusion. The unique features of the OcclusionChip device include the microfluidic anastomotic design preventing early upstream clogging, gradient microcapillary arrays (>40 000 microcapillaries, 10 to 4 μm in the AOI), and the capacity to process clinical samples at near-physiological hematocrit (20% *vs.* <1% in other recent studies).[37,39] The LN functionalization allows assessment of RBC adhesion in a microcapillary flow-mimicking environment and in a relatively large area for adhesion quantification (~32 mm^2 *vs.* <3 mm^2 in another recent study).[56] Therefore, analysis of blood samples with greater or lower adhesive potential is enabled. Notably, RBC adhesion in non-functionalized microchannels, which is non-specific, is negligible compared to that in LN-functionalized microchannels (Fig. 2C, <4% in average), proving the efficacy of our surface functionalization approach.

In SCD, exaggerated endothelial activation leads to loss of endothelium integrity, cell apoptosis and necrosis, and consequently exposure of ECM components such as LN.[43,57] As a result, abnormally adhesive sickle RBCs adhere on the vasculature through a LN-dependent mechanism, which contributes to disease pathophysiology in SCD.[58,59] Even though in this work, microchannel surface functionalization was carried out with LN, of note other endothelial-associated adhesive molecules can be used for other specific applications, such as the evaluation of novel targeted therapies in SCD. For example, it has been shown that P-selectin mediates sickle RBC adhesion to endothelium,[60] and a humanized antibody targeting at P-selectin developed by Novartis was recently approved by the FDA for SCD treatment. Therefore, a P-selectin-functionalized OcclusionChip assay could simultaneously measure both RBC-mediated microcapillary occlusion and RBC adhesion to P-selectin, for potential patient screening and monitoring.

Our data confirm the significantly elevated RBC adhesion and microcapillary occlusion, due to increased RBC membrane adhesiveness and decreased RBC deformability in people with SCD (Fig. 2E and F), which are in line with previous findings. SCT (HbAS) is the condition in which a subject inherits one HbS and one HbA gene from the parents, and therefore people with SCT have both HbS and HbA in their RBCs (normally the HbA level is greater than the HbS level).[61] It is estimated that in SCT, the US population is up to 2 million and worldwide approaches 300 million.[62] Although several studies have described sudden death in SCT,[63–65] it is still under debate whether SCT should be treated as a benign condition.[66–68] Moreover, it is still controversial whether SCT is directly responsible for morbidities (such as renal disease and atrial fibrillation),[69,70] as the underlying mechanisms are unclear. Recent efforts have clearly shown that the blood properties of

people with SCT differ from the healthy, *e.g.*, deoxygenation and dehydration can cause HbAS RBC sickling.[71,72] Further, Lu *et al.* showed that HbAS blood becomes more viscous with increased oxygen tension,[73] Zheng *et al.* showed that HbAS RBCs have greater shear modulus and viscosity than control RBCs,[74] and Tripette *et al.* showed that HbAS RBCs have a slightly but significantly smaller elongation index than control RBCs measured by ektacytometry under high shear stress (9.49, 16.87 and 30 Pa).[75] While previous studies have suggested that HbAS RBCs are less deformable than healthy RBCs, particularly at low oxygen levels, studies on vascular adhesion are relatively limited.[76] Here, our data show that, under normoxic conditions, HbAS RBCs caused negligible microcapillary occlusion (Fig. 2E), but slightly enhanced adhesion to LN compared to HbA-containing RBCs (Fig. 2F). These data suggest that HbAS RBCs are deformable enough to pass through narrow microcapillaries in the body under normoxic conditions and that HbAS-containing RBCs are more adhesive than healthy RBCs. The LN counterpart, BCAM/Lu, on sickle RBC membranes in SCD is well-known; however, this mechanism for HbAS RBC adhesion on LN is not confirmed.

The ARC and LDH are important hemolytic biomarkers that have been linked to disease severity,[77,78] and here they are associated with both the OI and RBC adhesion to LN (-Fig. 3A, B, G and H). In SCD, sickle RBCs are vulnerable to shear flow stress and hemolysis, which triggers release of microvesicles and cell-free hemoglobin.[79–81] We postulate that hemolysis leads to a decreased surface-to-volume ratio and disrupted cytoskeletal network in RBCs in SCD, which translates to observed enhanced microcapillary occlusion. In addition, in sickle RBCs, BCAM/Lu binds to the LN alpha 5 chain.[82,83] It is known that young low-density reticulocytes, released from the bone marrow due to hemolytic stress, adhere to LN in SCD primarily through a Lu/BCAM phosphorylation mediated mechanism,[84] not seen in high-density mature sickle RBCs.[85] Likely, adherent RBCs in our assay are primarily reticulocytes, although sickle mature RBCs can also adhere on LN (previously reported to be 80% to 90% less than reticulocytes).[11] Altogether, these data suggest clinical relevance for the present assay in SCD, in which the OI measures the impact of stiff sickle RBCs on microvascular occlusion, and RBC adhesion measures the potential of sickle reticulocytes and mature RBCs to attach to exposed sub-endothelial-like matrices, as seen in microvascular damage (Fig. 5). If portable and convenient (integrated with electrical measurement features for widespread use as previously described[86]), this assay has the potential to subtly monitor the clinical course in SCD.

In a single recipient of allogeneic HSCT, RBC samples before and after showed decreased adhesion and microcapillary occlusion (Fig. 4). Recently, the limitations of allogeneic HSCT such as infections, graft *versus* host disease (GVHD), graft rejection (GR), and limited myeloablative matched source have become evident.[87–89] Gene therapy can address, directly or indirectly, the underlying cause of SCD, where *ex vivo* gene transfer into or gene manipulation of autologous hematopoietic stem cells results in the addition of an anti-sickling hemoglobin (HbA^{T87Q}) or augmented induction of HbF.[90–92] In a recent study, RBC deformability was assessed by ektacytometry following gene therapy in a patient with SCD.[93] However, abnormal RBC adhesion to endothelial-associated markers was a missing piece. Our data show that following HSCT, the subject still exhibited RBC adhesion to LN beyond the healthy range (Fig. 4B), emphasizing the importance of simultaneous measurement of both RBC deformability and adhesiveness. The present assay could therefore supplement other clinical observations *i.e.* by measuring two functional hemorheological properties

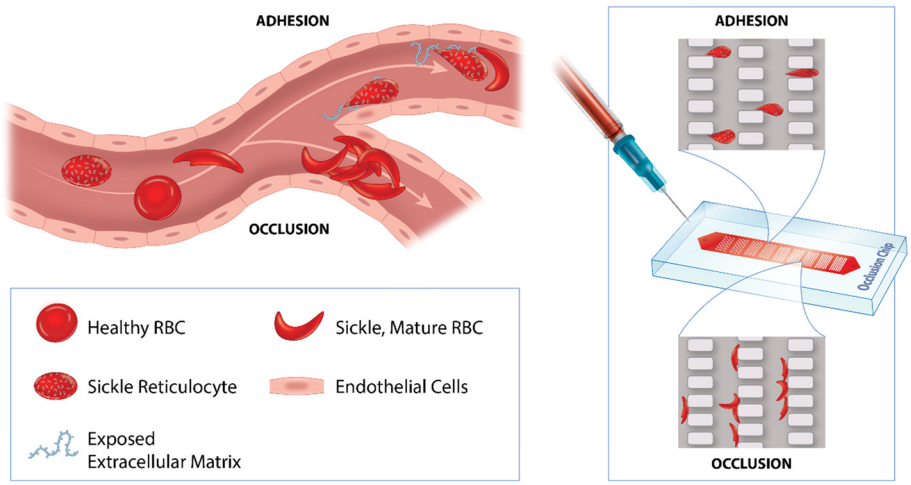

Fig. 5 Clinical significance of the present laminin (LN)-functionalized OcclusionChip assay. Enhanced red cell hemolysis in SCD, characterized by an elevated absolute reticulocyte count (ARC) and lactate dehydrogenase (LDH) level, results in decreased RBC deformability, increased circulating reticulocytes, and increased microvascular endothelial activation/damage, which translate into enhanced RBC adhesion and RBC-mediated microcapillary occlusion as measured in the present assay. Patients with enhanced vascular hemolysis are more transfused, ultimately leading to iron overload and an increased ferritin level in SCD (illustration credit: Grace Gongaware).

for a more comprehensive evaluation of the outcome of novel therapies, such as gene therapy.

There are limitations in this work. First, patient numbers are modest. Second, sickle reticulocyte and sickle mature RBC adhesion and sickling/occlusion profiles under normoxic or physiological hypoxic conditions were not measured here. For instance, our recent published study shows that sickle reticulocytes and sickle mature RBCs bear different adhesion characteristics under hypoxia, which is membrane-sulfatide dependent and varies from patient to patient.[94] Third, manual counting of RBC adhesive and occlusive events in the microchannel greatly hinders the OcclusionChip potential for clinical translation. Future work will prospectively focus on demonstrating the clinical utility of the functionalized OcclusionChip assay as an *in vitro* therapeutic benchmark in a larger patient population with homozygous SCD, under normoxic and hypoxic conditions, and monitoring diverse treatments including conventional, targeted, or curative therapies. Moreover, an artificial neural network (ANN) based machine learning algorithm for automated image analysis and cell counting also warrants future studies.

Author contributions

YM, DHW and RA contributed equally to this work. YM and UAG conceived the project. YM, DHW, RA, PW, KM and CF performed the experiments. YM, DHW, RA, PW, KM, UG, ZS and WJW analyzed the results. AB collected the patient clinical data. YM, DHW and RA prepared the figures and table, and wrote the manuscript. LVN, JAL and UAG reviewed and edited the manuscript. LVN provided the patient blood samples.

Conflicts of interest

A patent application has been filed by Case Western Reserve University for this technology.

Acknowledgements

This work was supported by the National Science Foundation (NSF) CAREER Award 1552782, and the National Heart, Lung, and Blood Institute (NHLBI) grants R01HL133574, R42HL162214, OT2HL152643, U01HL117659, T32HL134622 and K25HL159358. The authors acknowledge with gratitude the contributions of patients and clinicians at University Hospitals Cleveland Medical Center. The authors gratefully acknowledge the help from Patricia Conrad and Richard Lee at the Light Microscopy Imaging Core, Case Western Reserve University (CWRU). The authors gratefully acknowledge the help from Ina Martin at the Materials for Opto/electronics Research and Education (MORE) Center, CWRU. The authors acknowledge with gratitude Dr. Emily Pentzer at the Materials Science and Engineering Department, Texas A&M University for access to the ATR-FTIR spectrometer.

References

1 M. Bessis and G. Delpech, *Blood Cells*, 1981, **7**, 447–480.
2 R. S. Sprague, A. H. Stephenson and M. L. Ellsworth, *Trends Endocrinol. Metab.*, 2007, **18**, 350–355.
3 M. Leewenhoeck, *Philos. Trans. R. Soc.*, 1975, **10**, 380–385.
4 R. Huisjes, A. Bogdanova, W. W. van Solinge, R. M. Schiffelers, L. Kaestner and R. van Wijk, *Front. Physiol.*, 2018, **9**, 656.
5 V. Pretini, M. H. Koenen, L. Kaestner, M. H. A. M. Fens, R. M. Schiffelers, M. Bartels and R. Van Wijk, *Front. Physiol.*, 2019, **10**, 945.
6 N. Mohandas and P. G. Gallagher, *Blood*, 2008, **112**, 3939–3948.
7 G. A. Barabino, M. O. Platt and D. K. Kaul, *Annu. Rev. Biomed. Eng.*, 2010, **12**, 345–367.
8 D. K. Kaul, E. Finnegan and G. A. Barabino, *Microcirculation*, 2009, **16**, 97–111.
9 K. Sugihara, T. Sugihara, N. Mohandas and R. P. Hebbel, *Blood*, 1992, **80**, 2634–2642.
10 R. A. Swerlick, J. R. Eckman, A. Kumar, M. Jeitler and T. M. Wick, *Blood*, 1993, **82**, 1891–1899.
11 P. C. Hines, Q. Zen, S. N. Burney, D. A. Shea, K. I. Ataga, E. P. Orringer, M. J. Telen and L. V. Parise, *Blood*, 2003, **101**, 3281–3287.
12 M. M. Trinh-Trang-Tan, C. Vilela-Lamego, J. Picot, M. P. Wautier and J. P. Cartron, *Haematologica*, 2010, **95**, 730–737.
13 E. A. Evans, *Biophys. J.*, 1983, **43**, 27–30.
14 B. Gonzalez-Bermudez, G. V. Guinea and G. R. Plaza, *Biophys. J.*, 2019, **116**, 587–594.
15 N. Mohandas and E. Evans, *J. Clin. Invest.*, 1985, **76**, 1605–1612.
16 J. L. Maciaszek, K. Partola, J. Zhang, B. Andemariam and G. Lykotrafitis, *J. Biomech.*, 2014, **47**, 3855–3861.
17 I. Dulinska Molak, M. Targosz, W. Strojny, M. Lekka, P. Czuba, W. Balwierz and M. Szymonski, *J. Biochem. Biophys. Methods*, 2006, **66**, 1–11.
18 J. L. Maciaszek and G. Lykotrafitis, *J. Biomech.*, 2011, **44**, 657–661.
19 A. Li, A. H. Mansoor, K. S. W. Tan and C. T. Lim, *J. Microbiol. Methods*, 2006, **66**, 434–439.
20 M. M. Brandao, A. Fontes, M. L. Barjas-Castro, L. C. Barbosa, F. F. Costa, C. L. Cesar and S. T. Saad, *Eur. J. Haematol.*, 2003, **70**, 207–211.
21 S. Y. Hu, X. Gou, H. C. Han, A. Y. H. Leung and D. Sun, *J. Biomed. Nanotechnol.*, 2013, **9**, 281–285.
22 M. T. Inanc, I. Demirkan, C. Ceylan, A. Ozkan, O. Gundogdu, U. Goreke, U. A. Gurkan and M. B. Unlu, *RSC Adv.*, 2021, **11**, 15519–15527.
23 T. L. Berezina, S. B. Zaets, C. Morgan, C. R. Spillert, M. Kamiyama, Z. Spolarics, E. A. Deitch and G. W. Machiedo, *J. Surg. Res.*, 2002, **102**, 6–12.
24 C. D. Brown, H. S. Ghali, Z. H. Zhao, L. L. Thomas and E. A. Friedman, *Kidney Int.*, 2005, **67**, 295–300.
25 A. A. Khalili and M. R. Ahmad, *Int. J. Mol. Sci.*, 2015, **16**, 18149–18184.

26 M. A. E. Rab, C. K. Kanne, J. Bos, B. A. van Oirschot, C. Boisson, M. E. Houwing, J. Gerritsma, E. Teske, C. Renoux, J. Riedl, R. E. G. Schutgens, M. Bartels, E. Nur, P. Joly, R. Fort, M. H. Cnossen, R. van Wijk, P. Connes, E. J. van Beers and V. A. Sheehan, *Am. J. Hematol.*, 2021, **96**, E29–E32.
27 N. Z. Piety, J. Stutz, N. Yilmaz, H. Xia, T. Yoshida and S. S. Shevkoplyas, *Sci. Rep.*, 2021, **11**, 604.
28 N. L. Parrow, P. C. Violet, H. B. Tu, J. Nichols, C. A. Pittman, C. Fitzhugh, R. E. Fleming, N. Mohandas, J. F. Tisdale and M. Levine, *J. Visualized Exp.*, 2018, **131**, 59610.
29 Y. Man, R. An, K. Monchamp, Z. Sekyonda, E. Kucukal, C. Federici, W. J. Wulftange, U. Goreke, A. Bode, V. A. Sheehan and U. A. Gurkan, *Front. Physiol.*, 2022, **13**, 954106.
30 Y. Qiu, B. Ahn, Y. Sakurai, C. E. Hansen, R. Tran, P. N. Mimche, R. G. Mannino, J. C. Ciciliano, T. J. Lamb, C. H. Joiner, S. F. Ofori-Acquah and W. A. Lam, *Nat. Biomed. Eng.*, 2018, **2**, 453–463.
31 M. Tsai, A. Kita, J. Leach, R. Rounsevell, J. N. Huang, J. Moake, R. E. Ware, D. A. Fletcher and W. A. Lam, *J. Clin. Invest.*, 2012, **122**, 408–418.
32 E. Kucukal, A. Ilich, N. S. Key, J. A. Little and U. A. Gurkan, *Am. J. Hematol.*, 2018, **93**, 1050–1060.
33 P. Noomuna, M. Risinger, S. Zhou, K. Seu, Y. Man, R. An, D. A. Sheik, J. Wan, J. A. Little, U. A. Gurkan, F. M. Turrini, T. Kalfa and P. S. Low, *Br. J. Haematol.*, 2020, **190**, 599–609.
34 E. Kucukal, Y. Man, E. Quinn, N. Tewari, R. An, A. Ilich, N. S. Key, J. A. Little and U. A. Gurkan, *Blood Adv.*, 2020, **4**, 3688–3698.
35 Y. Man, E. Kucukal, S. Liu, R. An, U. Goreke, W. J. Wulftange, Z. Sekyonda, A. Bode, J. A. Little, D. Manwani, E. X. Stavrou and U. A. Gurkan, *Biosens. Bioelectron.*, 2023, **222**, 114921.
36 Y. Man, U. Goreke, E. Kucukal, A. Hill, R. An, S. Liu, A. Bode, A. Solis-Fuentes, L. V. Nayak, J. A. Little and U. A. Gurkan, *Blood Cells, Mol., Dis.*, 2020, **83**, 102424.
37 J. Picot, P. A. Ndour, S. D. Lefevre, W. El Nemer, H. Tawfik, J. Galimand, L. Da Costa, J. A. Ribeil, M. de Montalembert, V. Brousse, B. Le Pioufle, P. Buffet, C. Le Van Kim and O. Francais, *Am. J. Hematol.*, 2015, **90**, 339–345.
38 E. Du, M. Diez-Silva, G. J. Kato, M. Dao and S. Suresh, *Proc. Natl. Acad. Sci. U. S. A.*, 2015, **112**, 1422–1427.
39 E. Islamzada, K. Matthews, Q. Guo, A. T. Santoso, S. P. Duffy, M. D. Scott and H. Ma, *Lab Chip*, 2020, **20**, 226–235.
40 V. M. Dominical, D. M. Vital, F. O'Dowd, S. T. Saad, F. F. Costa and N. Conran, *Exp. Hematol.*, 2015, **43**, 223–228.
41 M. Lu, C. K. Kanne, R. C. Reddington, D. L. Lezzar, V. A. Sheehan and S. S. Shevkoplyas, *Front. Physiol.*, 2021, **12**, 633080.
42 Y. Man, E. Kucukal, R. An, Q. Watson, J. Bosch, P. A. Zimmerman, J. A. Little and U. A. Gurkan, *Lab Chip*, 2020, **20**, 2086–2099.
43 S. P. Lee, M. L. Cunningham, P. C. Hines, C. C. Joneckis, E. P. Orringer and L. V. Parise, *Blood*, 1998, **92**, 2951–2958.
44 Y. Man, E. Kucukal, R. An, A. Bode, J. A. Little and U. A. Gurkan, *Microcirculation*, 2021, **28**, e12662.
45 A. G. Hudetz, *Microcirculation*, 1997, **4**, 233–252.
46 J. P. Delaney, *Am. J. Physiol.*, 1969, **216**, 1556–1561.
47 S. Wang, M. Esfahani, U. A. Gurkan, F. Inci, D. R. Kuritzkes and U. Demirci, *Lab Chip*, 2012, **12**, 1508–1515.
48 Y. Alapan, C. Kim, A. Adhikari, K. E. Gray, E. Gurkan-Cavusoglu, J. A. Little and U. A. Gurkan, *Transl. Res.*, 2016, **173**, 74–91e78.
49 Y. Alapan, J. A. Little and U. A. Gurkan, *Sci. Rep.*, 2014, **4**, 7173.
50 Y. Alapan, Y. Matsuyama, J. A. Little and U. A. Gurkan, *Technology*, 2016, **4**, 71–79.
51 E. Kucukal, Y. Man, A. Hill, S. Liu, A. Bode, R. An, J. Kadambi, J. A. Little and U. A. Gurkan, *Am. J. Hematol.*, 2020, **95**, 1246–1256.
52 C. Yang, L. Diao and R. Cook, *Survival Prediction-Algorithms, Challenges and Applications*, 2021, pp. 83–94.
53 C. Yang, L. Diao and R. J. Cook, *Stat. Med.*, 2022, **41**, 4403–4425.
54 Y. Sheng, C. Yang, S. Curhan, G. Curhan and M. Wang, *Stat. Med.*, 2022, **41**, 5335–5348.
55 J. Liu, L. He, L. Wang, Y. Man, L. Huang, Z. Xu, D. Ge, J. Li, C. Liu and L. Wang, *ACS Appl. Mater. Interfaces*, 2016, **8**, 30576–30582.
56 K. R. Partola, B. Andemariam and G. Lykotrafitis, *J. Mech. Behav. Biomed. Mater.*, 2017, **71**, 80–84.
57 F. Dignat-George and J. Sampol, *Eur. J. Haematol.*, 2000, **65**, 215–220.
58 C. A. Hillery, M. C. Du, R. R. Montgomery and J. P. Scott, *Blood*, 1996, **87**, 4879–4886.
59 N. Conran, C. F. Franco-Penteado and F. F. Costa, *Hemoglobin*, 2009, **33**, 1–16.
60 N. M. Matsui, L. Borsig, S. D. Rosen, M. Yaghmai, A. Varki and S. H. Embury, *Blood*, 2001, **98**, 1955–1962.
61 P. Connes, O. Hue, J. Tripette and M. D. Hardy-Dessources, *Clin. Hemorheol. Microcirc.*, 2008, **39**, 179–184.
62 N. S. Key and V. K. Derebail, *Hematology Am. Soc. Hematol. Educ. Program*, 2010, **2010**, 418–422.
63 S. R. Jones, R. A. Binder and E. M. Donowho, Jr., *N. Engl. J. Med.*, 1970, **282**, 323–325.
64 J. A. Kark, D. M. Posey, H. R. Schumacher and C. J. Ruehle, *N. Engl. J. Med.*, 1987, **317**, 781–787.
65 D. P. Wirthwein, S. D. Spotswood, J. J. Barnard and J. A. Prahlow, *J. Forensic Sci.*, 2001, **46**, 399–401.
66 O. K. Baskurt, H. J. Meiselman and M. F. Bergeron, *J. Appl. Physiol.*, 2007, **103**, 2142.
67 P. Connes, M.-D. Hardy-Dessources and O. Hue, *J. Appl. Physiol.*, 2007, **103**, 2138.
68 D. Le Gallais, J. Lonsdorfer, P. Bogui and S. Fattoum, *J. Appl. Physiol.*, 2007, **103**, 2137.
69 E. S. Roach, *Arch. Neurol.*, 2005, **62**, 1781–1782.
70 G. Tsaras, A. Owusu-Ansah, F. O. Boateng and Y. Amoateng-Adjepong, *Am. J. Med.*, 2009, **122**, 507–512.
71 M. F. Bergeron, J. G. Cannon, E. L. Hall and A. Kutlar, *Clin. J. Sport Med.*, 2004, **14**, 354–356.
72 J. A. Kark and F. T. Ward, *Semin. Hematol.*, 1994, **31**, 181–225.
73 X. R. Lu, A. Chaudhury, J. M. Higgins and D. K. Wood, *Am. J. Hematol.*, 2018, **93**, 1227–1235.

74 Y. Zheng, M. A. Cachia, J. Ge, Z. Xu, C. Wang and Y. Sun, *Lab Chip*, 2015, **15**, 3138–3146.
75 J. Tripette, P. Connes, E. Beltan, T. Chalabi, L. Marlin, R. Chout, O. K. Baskurt, O. Hue and M. D. Hardy-Dessources, *Clin. Hemorheol. Microcirc.*, 2010, **45**, 39–52.
76 G. A. Barabino, L. V. McIntire, S. G. Eskin, D. A. Sears and M. Udden, *Blood*, 1987, **70**, 152–157.
77 T. M. Mikobi, P. L. Tshilobo, M. N. Aloni, G. M. Lelo, P. Z. Akilimali, J. J. Muyembe-Tamfum, V. Race, G. Matthijs and J. M. M. Mwamba, *PLoS One*, 2015, **10**, e0123568.
78 E. R. Meier, R. M. Fasano and P. R. Levett, *Blood Cells, Mol., Dis.*, 2017, **65**, 86–94.
79 D. M. Brunetta, G. C. De Santis, A. C. Silva-Pinto, L. C. Oliveira de Oliveira and D. T. Covas, *Acta Haematol.*, 2015, **133**, 287–294.
80 M. A. Lizarralde Iragorri, S. El Hoss, V. Brousse, S. D. Lefevre, M. Dussiot, T. Xu, A. R. Ferreira, Y. Lamarre, A. C. Silva Pinto, S. Kashima, C. Lapoumeroulie, D. T. Covas, C. Le Van Kim, Y. Colin, J. Elion, O. Francais, B. Le Pioufle and W. El Nemer, *Lab Chip*, 2018, **18**, 2975–2984.
81 R. An, Y. Huang, Y. Man, R. W. Valentine, E. Kucukal, U. Goreke, Z. Sekyonda, C. Piccone, A. Owusu-Ansah, S. Ahuja, J. A. Little and U. A. Gurkan, *Lab Chip*, 2021, **21**, 1843–1865.
82 W. El Nemer, P. Gane, Y. Colin, V. Bony, C. Rahuel, F. Galacteros, J. P. Cartron and C. Le Van Kim, *J. Biol. Chem.*, 1998, **273**, 16686–16693.
83 M. Udani, Q. Zen, M. Cottman, N. Leonard, S. Jefferson, C. Daymont, G. Truskey and M. J. Telen, *J. Clin. Invest.*, 1998, **101**, 2550–2558.
84 P. Bartolucci, V. Chaar, J. Picot, D. Bachir, A. Habibi, C. Fauroux, F. Galactéros, Y. Colin, C. Le van Kim and W. El Nemer, *Blood*, 2010, **116**, 2152–2159.
85 M. A. Lizarralde-Iragorri, S. D. Lefevre, S. Cochet, S. El Hoss, V. Brousse, A. Filipe, M. Dussiot, S. Azouzi, C. Le Van Kim, F. Rodrigues-Lima, O. Francais, B. Le Pioufle, T. Klei, R. van Bruggen and W. El Nemer, *Haematologica*, 2020, **106**, 2478–2488.
86 Y. Man, D. Maji, R. An, S. P. Ahuja, J. A. Little, M. A. Suster, P. Mohseni and U. A. Gurkan, *Lab Chip*, 2021, **21**, 1036–1048.
87 S. Shenoy, *Ther. Adv. Hematol.*, 2013, **4**, 335–344.
88 M. Bhatia and S. Sheth, *J. Blood Med.*, 2015, **6**, 229–238.
89 L. Krishnamurti, S. Abel, M. Maiers and S. Flesch, *Bone Marrow Transplant.*, 2003, **31**, 547–550.
90 K. Bourzac, *Nature*, 2017, **549**, S28–S30.
91 A. A. Thompson, M. C. Walters, J. Kwiatkowski, J. E. J. Rasko, J. A. Ribeil, S. Hongeng, E. Magrin, G. J. Schiller, E. Payen, M. Semeraro, D. Moshous, F. Lefrere, H. Puy, P. Bourget, A. Magnani, L. Caccavelli, J. S. Diana, F. Suarez, F. Monpoux, V. Brousse, C. Poirot, C. Brouzes, J. F. Meritet, C. Pondarre, Y. Beuzard, S. Chretien, T. Lefebvre, D. T. Teachey, U. Anurathapan, P. J. Ho, C. von Kalle, M. Kletzel, E. Vichinsky, S. Soni, G. Veres, O. Negre, R. W. Ross, D. Davidson, A. Petrusich, L. Sandler, M. Asmal, O. Hermine, M. De Montalembert, S. Hacein-Bey-Abina, S. Blanche, P. Leboulch and M. Cavazzana, *N. Engl. J. Med.*, 2018, **378**, 1479–1493.
92 V. G. Sankaran, T. F. Menne, J. Xu, T. E. Akie, G. Lettre, B. Van Handel, H. K. A. Mikkola, J. N. Hirschhorn, A. B. Cantor and S. H. Orkin, *Science*, 2008, **322**, 1839–1842.
93 J. A. Ribeil, S. Hacein-Bey-Abina, E. Payen, A. Magnani, M. Semeraro, E. Magrin, L. Caccavelli, B. Neven, P. Bourget, W. El Nemer, P. Bartolucci, L. Weber, H. Puy, J. F. Meritet, D. Grevent, Y. Beuzard, S. Chretien, T. Lefebvre, R. W. Ross, O. Negre, G. Veres, L. Sandler, S. Soni, M. de Montalembert, S. Blanche, P. Leboulch and M. Cavazzana, *N. Engl. J. Med.*, 2017, **376**, 848–855.
94 U. Goreke, E. Kucukal, F. Wang, R. An, N. Arnold, E. Quinn, C. Yuan, A. Bode, A. Hill, Y. Man, B. C. Hambley, R. Schilz, M. Ginwalla, J. A. Little and U. A. Gurkan, *Blood Adv.*, 2023, DOI: **10.1182/bloodadvances.2022008392**.